Since January 2020 Elsevier has created a COVID-19 resource centre with free information in English and Mandarin on the novel coronavirus COVID-19. The COVID-19 resource centre is hosted on Elsevier Connect, the company's public news and information website.

FUTURE PROSPECTS

By MICHAEL G. ROSSMANN, ANTHONY J. BATTISTI, AND PAVEL PLEVKA

Department of Biological Sciences, Purdue University, West Lafayette, Indiana, USA

Abstract

Cryo-electron microscopy (cryo-EM) in combination with single-particle analysis has begun to complement crystallography in the study of large macromolecules at near-atomic resolution. Furthermore, advances in cryo-electron tomography have made possible the study of macromolecules within their cellular environment. Single-particle and tomographic studies will become even more useful when technologies for improving the signal-to-noise ratio such as direct electron detectors and phase plates become widely available. Automated image acquisition has significantly reduced the time and effort required to determine the structures of macromolecular assemblies. As a result, the number of structures determined by cryo-EM is growing exponentially. However, there is an urgent need for improved criteria for validating both the reconstruction process and the atomic models derived from cryo-EM data. Another major challenge will be mitigating the effects of anisotropy caused by the missing wedge and the excessively low signal-to-noise ratio for tomographic data. Parallels between the development of macromolecular crystallography and cryo-EM have been used to tentatively predict the future of cryo-EM.

ADVANCES IN PROTEIN CHEMISTRY AND STRUCTURAL BIOLOGY, Vol. 82
DOI: 10.1016/B978-0-12-386507-6.00005-1

I. Introduction: History of Structural Biology and the Increasing Importance of Electron Microscopy

The growing numbers of cryo-electron microscopy (cryo-EM) and cryo-electron tomography (cryo-ET) reconstructions deposited with the Protein Data Bank (PDB) (Fig. 1) indicate that these methods have become frequently used techniques for determining structures of macromolecular complexes. Nevertheless, X-ray crystallographic structure determinations

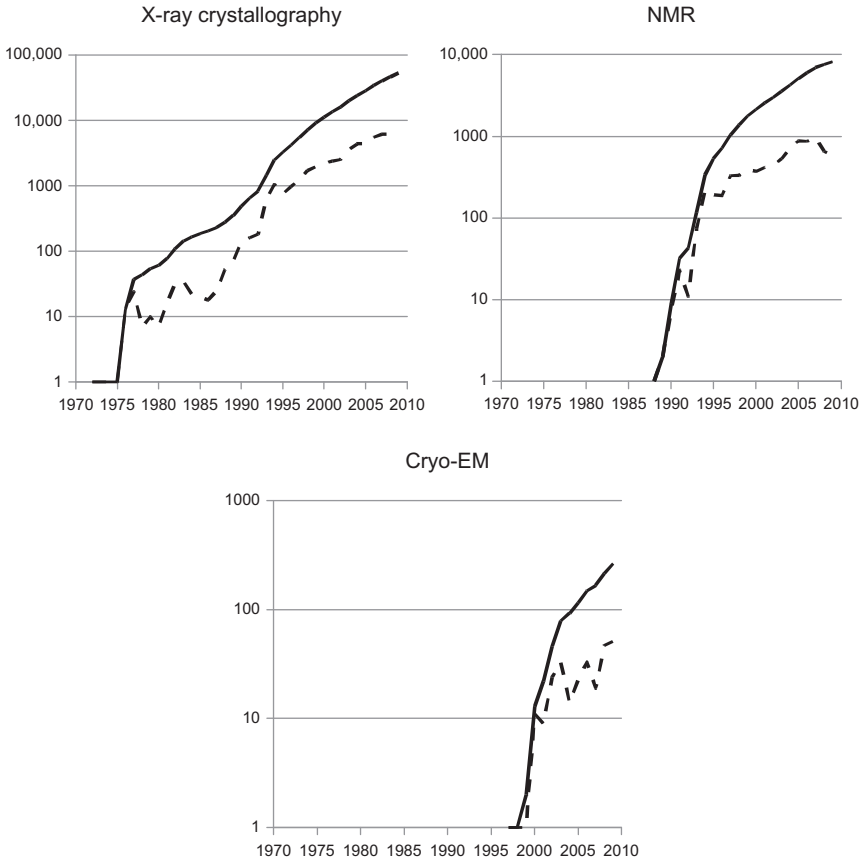

Fig. 1. *Number of structures deposited with the Protein Data Bank*. The dashed line represents the number of structures deposited in a given year. The solid line represents the total number of deposited structures. Source: RCSB-PDB.

still dominate both electron microscopy (EM) and NMR spectroscopy. Because X-ray crystallography has had the longest history, the initial part of this chapter will trace the development of macromolecular crystallography and compare it with the more recent development of cryo-EM in order to extrapolate and divine the future of this latest tool of structural biology.

In 1912 in Munich, Germany, Paul Ewald, together with two students, W. Friedrich and P. Knipping, demonstrated that a crystal of Cu_2SO_4 could diffract X-rays, consistent with von Laue's predictions (Ewald, 1962). The experiment was performed at night to avoid the wrath of the senior professors who were of the opinion that the experiment was worthless. Yet, this small episode changed science and the world. Less than 50 years later, the same technology had been used to determine the first atomic structures of two proteins (Kendrew et al., 1958; Kendrew et al., 1960; Perutz et al., 1960; Hadfield et al., 1995), and by the time another 25 years had gone by the structure of two human viruses had been determined (Hogle et al., 1985; Rossmann et al., 1985). Even more recently, the structure and mechanism of the protein synthesizing ribosomal machine (http://nobelprize.org/nobel_prizes/chemistry/laureates/2009/) were established. From its beginning, X-ray crystallography was a method that was capable of resolving individual atoms, but its power to view large, complex biological molecules grew only gradually. By the end of the twentieth century, pharmaceutical companies were eagerly employing crystallographers in the hopes that structural information would lead to cures for numerous human diseases. Yet, just like a financial bubble, the good times are now coming to an end, as the proteins whose structures have not yet been determined are ever more difficult to crystallize. The projects have grown more ambitious, aiming at membrane proteins and large protein complexes. Fortunately, EM has now advanced to a point where it is rapidly replacing crystallography as the major pioneering tool of structural biology (Harrison, 2010).

The 1912 experiment showed that X-rays were waves, that the repeating units in crystals were of roughly the same dimensions as the wavelength of X-rays, and confirmed the chemical ideas of the atomicity of matter. This news spread rapidly to England where Lawrence Bragg interpreted the mathematical expressions of von Laue to an easier to comprehend physical concept. He went on to use his physical insight to show that the pattern of intensities caused by the diffraction of X-rays from crystals of NaCl and KCl were consistent with spherical metal ions filling the spaces between

the larger spherical, cubic close packed, Cl^- ions (Bragg, 1913). Chemists of the time found this difficult to comprehend as they thought that NaCl was a compound consisting of individual NaCl molecules. When eventually the heated discussion was settled in favor of the cubic arrangement of ions, this discovery turned out to be the birth of structural chemistry. After the end of the First World War in 1918, there reemerged an interest in structural crystallography, led by Sir Lawrence Bragg. Initially, this was directed to the investigation of centric structures, mainly minerals, many of which had interesting symmetries, but gradually crystallographers turned to organic compounds. For instance, Kathleen Lonsdale (later to be elected the first female Fellow of the Royal Society) was able to confirm that hexamethylbenzene was a flat molecule (Lonsdale, 1928). Notwithstanding the difficulties of the Second World War, Dorothy Crowfoot Hodgkin had been able to establish the structure of the asymmetric penicillin molecule, the first antibiotic used with much success during the Second World War (Crowfoot, 1948).

By this time, crystallographers had gone beyond the ''trial and error'' approach of guessing at atomic positions and were starting to use a variety of computational tools including the Patterson function (Patterson, 1934, 1935) and the heavy atom technique. In addition, crystallographers had discovered the use of Fourier syntheses to represent electron density as presented on stacked sheets of glass plates (Bragg, 1929). These new techniques required lengthy calculations, helped by such tools as Beevers Lipson ''strips'' (Beevers and Lipson, 1936) for the manual summation of a Fourier series. Fortunately, the first home-built, and then commercial, electronic computers became available in the 1950s. Many of the early crystallographic structures had been determined with only one- or two-dimensional data, but with the advent of better computational devices there was a desire to extend data collection into three dimensions. This set the stage, as mentioned above, for the structural determinations of biological macromolecules and molecular assemblies in the second half of the twentieth century. The structure determinations of large molecules also required large machines, such as robots, for producing crystals, synchrotrons to produce intense, coherent, almost monochromatic X-rays, and fast computer graphics piggy-backed on the development of gaming machines. The most recent emphasis has been on ever-smaller crystals, as the difficulty of growing crystals has increased in proportion to the size of the object being crystallized. In some experiments, the crystals

are only a few unit cells in each direction, while others have been even more audacious by looking at the diffraction pattern of single molecules (Bogan et al., 2008) with the help of extremely intense X-ray lasers (Kirian et al., 2010). Indeed, the increasing demands on instrumentation are pushing X-ray imaging techniques to the limits of what is achievable (Rossmann and Arnold, 2001). There are, however, alternative simpler and less expensive ways for obtaining structural results at the boundaries of structural biology.

X-ray detectors measure only intensities, from which the amplitude of the diffracted rays can be evaluated. The relative phase of the diffracted rays is the central ''phase problem'' of any X-ray structure determination. The phases need to be determined indirectly in order to be able to calculate the electron density distribution in the crystal. In contrast, an electron microscope uses the wave properties of the electrons to form an image of the object in the same way as does a light microscope. Unlike X-rays, scattered electrons can be focused with magnetic lenses, allowing an image to be formed and thereby solving the phase problem directly. The average wavelength of fast electrons is around 0.02 Å, of X-rays roughly 1 Å, compared to 3900–7500 Å for visible light. Thus, unlike visible light, electrons and X-rays can be used to resolve individual atoms (covalently bonded atoms are separated by about 1.5 Å). Nevertheless, the development of atomic-resolution EM has lagged behind the development of X-ray crystallography.

The first electron microscope was constructed by Ernst Ruska in 1931. This was a time of rapid advances in basic physics when the properties of elementary particles were being debated. However, the early microscopes were not much of an advance on light microscopes and had the additional disadvantage of requiring the specimen to be in a vacuum. Development accelerated after the end of the Second World War with the introduction of negative stains using heavy metal dyes to enhance contrast between water and the almost equally dense biological samples. Unfortunately, the staining process also caused distortions and artifacts in the samples.

De Rosier and Klug (1968) suggested combining different projections of isolated molecular particles in order to create a three-dimensional image. This led to the three-dimensional structure determinations of small plant viruses using negatively stained samples (Crowther and Amos, 1972). An important breakthrough came in 1988 with the use of flash freezing techniques for embedding the specimen in vitreous

(amorphous) ice (Dubochet et al., 1988). This technique preserved the specimen in a near-native state, free of the artifacts of staining. Immediately, there was a flurry of new reconstructions, particularly of viruses but also of ribosomes, chaperones, and other molecular assemblies. Large complexes that could not be crystallized, such as viruses interacting with cellular receptors (Olson et al., 1993) or viruses interacting with antibodies (Smith et al., 1993; Wikoff et al., 1994), could now be studied by combining cryo-EM of the complex with crystallography of the individual component molecules (Rossmann, 2000; Rossmann et al., 2001) to generate ''pseudo-atomic'' models. Cryo-EM was used to obtain the lower resolution ''large picture'' into which the higher resolution crystal structures of the components were fitted (Rossmann, 2000; Rossmann et al., 2001), enabling analysis of interactions between the component structures. Another use of cryo-EM structures can be to provide a low-resolution model for molecular replacement to initiate X-ray crystal structure determinations by means of phase extension, as was the case for a ribosomal subunit (Ban et al., 1998) or phiX174 virus particle (Dokland et al., 1998). In contrast to X-ray crystallography, cryo-EM was initially used primarily to study complex homogeneous objects at rather limited resolution.

Another milestone was passed in 1998 with the subnanometer structure of hepatitis B cores determined by two independent groups (Böttcher et al., 1997; Conway et al., 1997). In the past 2 or 3 years, cryo-EM has been able to produce, in favorable cases, three-dimensional images that are comparable to X-ray crystal structures of icosahedral viruses (Jiang et al., 2008; Zhang et al., 2010). That has been an important development as it has become apparent that larger viruses with lipid envelopes cannot usually be crystallized or give only very poorly diffracting crystals (Harrison et al., 1992; Bamford et al., 2002; Kaufmann et al., 2010). But, like crystallography, this form of cryo-EM is also reaching its limits because large biological objects tend to be heterogeneous. For this reason, cryo-ET is becoming a more frequently used tool (Förster et al., 2005; Lučić et al., 2005). In this technique, a three-dimensional image is created by combining many images taken of the same sample oriented by a succession of tilt angles about a common axis (or multiple axes). Because the same sample is repeatedly exposed to the electron beam, the electron dose per image has to be kept very low to avoid radiation damage, lowering the feasible resolution. Currently, numerous schemes are being developed to mitigate the effects of the low dose, the physical limitations of the tilting

equipment, and the increased specimen thickness with increased tilt angle. These techniques are making inroads not only for the study of large heterogeneous molecular assemblies but also for bacteria and eukaryotic cells (Lučić et al., 2005).

II. The Beginnings of Cryo-Electron Tomography

De Rosier and Klug proposed two methods for rendering objects in three dimensions using transmission EM (De Rosier and Klug, 1968). One approach involved combining several images of randomly oriented particles and has evolved into what is now known as the ''single-particle method.'' The other proposed technique is much like modern-day electron tomography (ET), as it involved obtaining a series of sequentially tilted images. Although the single-particle method requires homogeneity of the macromolecules under study, the method using sequential tilts is applicable to unique structures.

Series of tilted micrographs were used to generate three-dimensional reconstructions of macromolecules beginning in the late 1960s and early 1970s (Hart, 1968; Hoppe et al., 1974), but acquiring a series of tilted images was an immense technical challenge at the dawn of the digital age, and development of this technique remained slow for decades. Progress was further hindered because applying doses greater than 1 $e^{-}/Å^{2}$ to the same portion of a specimen (Unwin and Henderson, 1975), as would be required for a tilted series, would destroy high-resolution information. Thus, tomography was not viewed as a viable method for obtaining reliable three-dimensional structures of macromolecules, and was therefore restricted to the examination of larger cellular components (Frank, 2006).

Unlike the sequential tilt method, single-particle methods enjoyed rapid development after 1968, and have been immensely successful in the study of large symmetric or asymmetric homogeneous macromolecules (Crowther et al., 1970; Frank, 1989). Single-particle studies rely upon averaging between a number of macromolecules which sit in random orientations, eliminating the technical difficulties associated with specimen tilting. It is also possible to limit the electron dose, as it is not necessary to repeatedly expose the same portion of the specimen. However, because this technique relies upon the assumption of particle homogeneity, it is limited in its application. Structural biology has largely ignored truly unique or heterogeneous molecules until the rebirth of the tilt series and ET

following the introduction of automated image acquisition (Koster et al., 1992), the availability of affordable CCD cameras, and the use of cryo-microscopy (Dubochet et al., 1988), which limits specimen beam damage and preserves the specimen in a near-native state.

There are still several technical limitations that make cryo-ET a relatively low-resolution tool when compared to X-ray crystallography or even single-particle cryo-EM. However, cryo-ET not only allows the analysis of heterogeneous structures, but it can also be used to study macromolecules within their cellular context.

III. Successes in Cryo-Electron Tomography

Cryo-ET has been a useful tool for the study of heterogeneous animal viruses. Harris et al. achieved a resolution at which the hemagglutinin (HA) and neuraminidase (NA) glycoprotein spikes can be distinguished in tomographic reconstructions of pleomorphic influenza virions (Harris et al., 2006). By fitting the known HA and NA structures into the tomographic densities, three-dimensional models were built showing the distribution of spikes on the influenza virion surface. Cryo-ET has also enabled structural studies of HIV core assembly (Briggs et al., 2006) as well as provided the first *in situ* structures of the trimeric spikes of HIV and other retroviruses (Förster et al., 2005; Zanetti et al., 2006; Zhu et al., 2006). Cryo-ET has also provided the first insights into the three-dimensional structures of intact coronaviruses (Bárcena et al., 2009), bunyaviruses (Freiberg et al., 2008; Overby et al., 2008; Huiskonen et al., 2010), poxviruses (Cyrklaff et al., 2005), and paramyxoviruses (Loney et al., 2009), all of which are known to cause serious disease in humans. Nevertheless, there are technical issues that need to be overcome before the structures of pleomorphic viruses approach the resolution of icosahedral viruses studied by single-particle or crystallographic methods.

The goals of structural biology do not involve only the determination of macromolecular structures to the highest possible resolution, but rather an investigation of these molecules within the context of the cell. To this end, Baumeister and coworkers have pioneered methods for the identification and mapping of macromolecules such as proteasomes and ribosomes within tomographically imaged cells (Frangakis et al., 2002; Medalia et al., 2002; Ortiz et al., 2006). As the library of macromolecular structures grows, so will increase the knowledge of the interactions among the components of

the cell. This might be achieved by using the library of cellular component structures to interpret tomograms of whole cells in a way analogous to the use of molecular folds in crystallographic molecular replacement. The large size of eukaryotic cells is an obstacle that limits the applicability of cryo-ET. However, with improvements in cryo-sectioning techniques (Leis et al., 2009), larger, more complicated cells can be rendered three-dimensionally.

Another potential use of ET is the identification of symmetry elements. For instance, Freiberg et al. extracted a number of Rift Valley fever virions from tomograms, some of which could then be aligned and averaged without any assumption of symmetry (Freiberg et al., 2008). Self-rotation functions (Tong and Rossmann, 1997) of the averaged density showed the presence of icosahedral symmetry, for a virus previously thought to be pleomorphic. Similar analysis could also be used to study objects that possess some local symmetry.

IV. Radiation Damage and the Missing Wedge

One obstacle in cryo-ET is the limited range of the tilted images, which results in a ''missing wedge'' of data. A second obstacle is the electron sensitivity of biological specimens that requires the electron dose to be minimized, resulting in a low signal-to-noise ratio. These problems can be alleviated in some situations by averaging homogeneous structures or by the application of symmetry. For example, Huiskonen et al. have used cryo-ET to observe that the Gn-Gc spikes on the surface of Tula hantavirus are tetrameric and are arranged into localized arrays (Hepojoki et al., 2010; Huiskonen et al., 2010). The spikes were then extracted from the tomogram and iteratively aligned and averaged to generate a structure of the spike to an isotropic resolution of 3.5 nm. The averaged spike was reintroduced into the original tomogram to give a global distribution of the spikes within the membrane.

One approach to reduce the size of the missing wedge has involved the use of dual-axis tomography (Iancu et al., 2005). Alternatively, embedding a specimen in rod-shaped vitreous ice could be used to generate a reconstruction without a systematic region of missing data and without the specimen thickening issues that occur with slab geometry. Rod-like specimens have previously been explored (Heymann et al., 2006; Kawase et al., 2007;

Hayashida et al., 2010), but achieving such a geometry with a frozen-hydrated specimen will likely prove to be more of a challenge. Kreysing et al. (2008) have developed an optical trap in which large eukaryotic cells can be rotated about a chosen axis and imaged with a light microscope. If a similar tool could be operated within a transmission electron microscope, objects could be rendered with isotropic resolution at the nanometer scale.

An alternative approach to transmission ET is ion-abrasion scanning EM (Heymann et al., 2006, 2009), in which a focused ion beam is used to ablate a fraction of the surface of a specimen that is subsequently imaged with scanning EM. Repeating this process leads to a stack of images that represent the three-dimensional structure of the object. The resolution limit for this technique is comparable to that of transmission ET ($\sim$6 nm in-plane and $\sim$20 nm in depth). If methods were developed to ablate the surface of a specimen in more finite increments than approximately 20 nm, such a technique would allow entire cells to be rendered in three dimensions in an isotropic fashion. Applying this technique to frozen-hydrated specimens requires further development.

Cryo-negative staining has been introduced as a means to improve the signal-to-noise ratio of projected images as well as provide further protection against radiation damage above and beyond traditional cryo-EM (Adrian et al., 1998; De Carlo et al., 2002). However, this technique has not yet achieved widespread usage in cryo-ET because the penetration of the stain may not be uniform throughout the specimen. Furthermore, cryo-negative staining may not preserve fine structural details and has been shown to dissociate the subunits of some specimens (De Carlo and Harris, 2010).

A phase plate inserted in the back-focal plane of the objective lens is capable of shifting the phase of the diffracted electron beam by $\pi/2$, changing the contrast transfer function from a sine-like to a cosine-like function. This allows the electron microscope to be operated close to focus. Under these conditions, the contrast transfer function is maximal at low resolution and the first node of the contrast transfer function occurs at a much higher resolution. Initial results have indicated improved signal-to-noise ratios for both single-particle and tomographic data (Murata et al., 2010). However, contamination of the phase plate can affect the phase shift. This issue will need to be overcome before phase plates are commonplace (Danev et al., 2009).

V. High-Resolution Cryo-EM Reconstructions

Recently, there have been some notable successes in determining structures of icosahedral viruses to a resolution that is high enough to enable model building based solely on the cryo-EM map, the amino acid sequence, and geometric constraints (Yu et al., 2008; Harrison, 2010; Liu et al., 2010a, 2010b; Zhang et al., 2010). Obtaining near-atomic-resolution results for less symmetric or asymmetric objects will require a proportionate amount of additional projection images, making experimental data collection daunting. Zhang et al. (2010) used approximately 2×10^4 virus particles to determine the structure of aquareovirus to 3.3 Å resolution using both icosahedral averaging and 10-fold averaging among quasi-equivalent subunits within the icosahedral asymmetric unit. An additional advantage of built-in icosahedral symmetry is that the relative orientations of 60 symmetrically related orientations are known exactly for each particle, whereas the relative orientations of asymmetric particles are subject to experimental error. Thus, obtaining a reconstruction with comparable resolution for an asymmetric object of similar size would require at least 1.2×10^7 particle images. Another obstacle to high-resolution structure determination is sample heterogeneity due to varying conformations of molecular assemblies. Although this can be tackled by the careful selection of images that correspond to closely related structures (Scheres et al., 2007), the need for additional data increases proportionately. Improving the resolution in these difficult cases will require efficient data acquisition techniques. The development of the LEGINON software for automated data collection marks a significant achievement in this area (Suloway et al., 2005). The use of charge-coupled device (CCD) detectors instead of films further expedites the data collection process (Clare and Orlova, 2010). Currently, in development are ''direct detectors'' that produce images with an improved signal-to-noise ratio by avoiding the conversion of electrons into photons required for CCD detectors (Milazzo et al., 2010).

Collection of protein X-ray diffraction patterns used to be a major challenge, sometimes requiring years to obtain a full data set. Now, with dedicated synchrotron radiation sources, only a few hours are required to collect complicated multiple wavelength data sets. Similarly, it is anticipated that future cryo-EM data acquisition will be much faster and less labor intensive. With improved data collection devices and improved computational techniques to classify heterogeneous samples, it may

become possible to observe dynamic processes. In the future, it may be possible to place an enzyme–substrate mixture into a microscope and obtain a movie describing the reaction mechanism in atomic detail.

VI. Molecular Models Derived from Cryo-EM Reconstructions

One goal of structural biology is the determination of molecular models that can be interpreted with respect to their function. Because macromolecular complexes can be difficult to crystallize, it is sometimes easier to determine the structure of the individual components of the complex. However, structures of individual proteins may not be sufficient for functional interpretation of molecular interactions in the absence of knowledge of their spatial relationships. Further, the structural details of component proteins within functionally relevant complexes are likely to differ in detail from individually determined structures. Cryo-EM maps of such complexes, though not yet typically determined to atomic resolution, can be interpreted at near-atomic resolution using ''pseudo-atomic'' models. In current practice, these models are constructed by rigid-body fitting of component structures, previously determined by X-ray crystallography or NMR (Cheng et al., 1995), into cryo-EM maps. The models are either treated as a single rigid body or split into a few domains that are each fitted separately (Zhang et al., 2004; Hafenstein et al., 2007; Cherrier et al., 2009). This approach is based on the observation that conformational changes of proteins are usually limited to the relative positioning of domains whose tertiary structure remains much the same.

At low resolution, the number of parameters that can be refined might be merely the orientation and position of a known three-dimensional rigid structure. However, as the resolution of the cryo-EM map improves, it may be possible to refine the orientation and position of individual structural elements such as α-helices and β-sheets. Finally, as the resolution improves beyond 4 Å, it becomes possible to refine Ramachandran and rotary dihedral angles, as is usually the case for a crystallographic refinement. Care must be taken that the number of parameters describing the structure is appropriate to the number of experimental measurements. For instance, the molecular structure of a eukaryotic ribosome (Taylor et al., 2009) was determined by combining a 7-Å cryo-EM reconstruction with molecular dynamics. The results are impressive given the complexity of

the structure. Nevertheless, such a structural determination requires validation, as the number of parameters describing the structure might be larger than the number of independent observations.

VII. Development of Validation Criteria

At this time, there is no set of tools that adequately describes either the quality of a cryo-EM reconstruction or the accuracy of the resultant model. The only criterion reported for most cryo-EM maps is the estimated resolution based on the Fourier Shell Correlation between two randomly selected half-sets. Whereas most papers estimate the resolution by the point at which the correlation falls below 0.5 (Böttcher et al., 1997; van Heel and Schatz, 2005), it has been suggested that this coefficient should be 0.143 (Rosenthal and Henderson, 2003) if the estimate of the resolution is to be compared to that of a crystallographic map. Standard methods to evaluate the quality and validity of cryo-EM reconstructions need to be developed and accepted. Also needed are criteria evaluating the molecular properties of the model as well as measures describing how well the model represents the cryo-EM map.

To evaluate quality of the cryo-EM reconstruction, a series of indicators should be developed documenting the whole pathway from data acquisition to calculation of the final model similar to current practices in crystallography. Thus, there should be indicators describing the quality of the collected images (similar to crystallographic R_{merge}; Rossmann et al., 1979), the accuracy of the contrast transfer function (CTF) determination for each image, and the accuracy of the particle orientation determination. Further statistics should describe the resulting map—What is its resolution ($I/\sigma(I)$ as a function of resolution)? How well does the map correspond to original experimental images (Baker et al., 1999)? Perhaps some of the experimental images could be excluded from the calculation of the reconstruction and used as a test set for an unbiased validation of the final map ($R_{\text{free}}^{\text{map}}$) (Brünger, 1992).

The fitting of atomic structures into cryo-EM maps for the purpose of evaluating pseudo-atomic models can be accomplished by the equivalent of a six-dimensional search. Whether an unambiguous solution can be found will depend on whether the best fit is significantly better than all other fits. However, if this is not the case, additional chemical and physical criteria can be used to identify the best fit (Rossmann et al., 2001). Once a reasonable fit has been obtained, the number of refinable parameters that describe the atomic model needs to be chosen according to the resolution

of the map. A parameter analogous to the crystallographic R_{free}^{model} would be a suitable measure to validate that the number of parameters does not exceed what is useful (Brünger, 1992).

Once an initial position and orientation of the model has been determined, it will be necessary to determine the accuracy of the parameters that describe the position of the model within the cryo-EM map (Rossmann et al., 2001; Volkmann and Hanein, 2003; Volkmann, 2009). The uncertainty in model fitting could be expressed by considering the various possible conformational changes that fit the observed data equally well. Such a multitude of conformations might be separately reported or can be represented as a ''temperature'' factor that describes the root mean square displacement of each atom from the mean, analogous to crystallographic practices. The knowledge of the error in the parameters will establish the validity of the subsequent interpretations.

When it is deemed possible to refine the individual atomic coordinates, statistics describing how well the refinement procedure preserved the geometric properties of the model should be given, including the Ramachandran plot distribution and the deviation of angles and bond lengths from their average values. Hopefully, the cryo-EM community will not repeat the history of protein crystallography in the 1990s when almost all models were described by their authors as ''better than average'' (Kleywegt and Jones, 1995).

To forecast the development of the validation criteria for cryo-EM, parallels with X-ray crystallography can be drawn. The crucial X-ray structure validation criteria R_{free} was introduced in 1992 (Brünger, 1992). By that time, the PDB archive contained approximately 650 structures (Fig. 1). It took several more years before the R_{free} and other structure validation criteria became generally applied and accepted (Kleywegt and Jones, 1995). The number of deposited cryo-EM structures will reach 650 in 2–3 years time. Thus, it should be expected that universally accepted validation criteria will soon be developed.

VIII. Data Deposition Policy

The future of cryo-EM will almost certainly bring an obligatory model and data deposition policy analogous to that now widely practiced for X-ray crystallography. The PDB was established in 1971, 13 years after

determination of the first X-ray structure of myoglobin in 1958 (Kendrew et al., 1958). By 1974, there had been 12 deposited structures. Since then, the number of entries has grown exponentially (Fig. 1). Initially, the X-ray structure deposition was not an obligatory prerequisite for publication of the results and only over time did it become a general requirement enforced by journal policies. It was only in 2008 that experimental data deposition became an obligatory component of atomic coordinate deposition to the PDB. The first model based on cryo-EM reconstruction was deposited with the PDB in 1997. Since then, the number of deposited models has grown exponentially and will be expected to be around 320 by the end of 2010 (Fig. 1). It will probably not be long until cryo-EM reconstruction deposition is generally mandated for publication. Based on the rate of crystallographic structures accumulated by the PDB, the rate of deposition of cryo-EM reconstructions is likely to continue growing exponentially for about a decade.

IX. Extrapolate into the Future

It would have been interesting to see Michael Faraday's reaction had somebody predicted that electromagnetic radiation would be used 150 years hence for instantaneously locating an acquaintance on the opposite side of the Earth, and then holding a casual conversation face-to-face as if both individuals were in the same room. Surely, Faraday would have laughed at what he would have thought to be just a silly joke. Similarly, predictions of future technical developments that are more than a lifetime ahead are likely to fall on deaf ears, but that is the task given to the authors of this chapter.

The technology of structural biology is changing rapidly. Crystallography, cryo-EM, and cryo-ET are becoming automatic, but maybe someday a single technique will supersede all current tools. Perhaps a tunable laser that can examine structure at all levels of detail, covering a resolution from 1 m to 0.1 nm will become available. Further, much progress will have been made to quickly gather large amounts of data and render structures in three dimensions almost instantaneously. For instance, all structural data on one hepatic cell might be collected within minutes. The automatic interpretation of the cell structure would then yield everything from the overall organization of the nucleus, cytoplasm, plasma membrane, and so forth, down to the positions of all atoms within every molecule in the

cell. This could be repeated numerous times in order to determine the dynamic properties of the cell. Clearly, such achievements will be an enormous boon for understanding molecular interactions and following the life cycle of individual cells. The effect of medication on the cell will be determined at the blink of an eye, allowing immediate correction of dosage. Such structural monitoring will become the passion of every doctor.

Acknowledgments

We thank Sheryl Kelly for her help in preparation of this chapter. Writing of this chapter was made possible by support from NIH (R01 AI11219, R01 AI76331, and P01 AI45976) and NSF (MCB-1014547) grants to M. G. R.

References

Adrian, M., Dubochet, J., Fuller, S. D., Harris, J. R. (1998). Cryo-negative staining. *Micron* **29**, 145–160.

Baker, T. S., Olson, N. H., Fuller, S. D. (1999). Adding the third dimension to virus life cycles: three-dimensional reconstruction of icosahedral viruses from cryo-electron micrographs. *Microbiol. Mol. Biol. Rev.* **63**, 862–922.

Bamford, J. K. H., Cockburn, J. J. B., Diprose, J., Grimes, J. M., Sutton, G., Stuart, D. I., et al. (2002). Diffraction quality crystals of PRD1, a 66-MDa dsDNA virus with an internal membrane. *J. Struct. Biol.* **139**, 103–112.

Ban, N., Freeborn, B., Nissen, P., Penczek, P., Grassucci, R. A., Sweet, R., et al. (1998). A 9 Å resolution X-ray crystallographic map of the large ribosomal subunit. *Cell* **93**, 1105–1116.

Bárcena, M., Oostergetel, G. T., Bartelink, W., Faas, F. G. A., Verkleij, A., Rottier, P. J. M., et al. (2009). Cryo-electron tomography of mouse hepatitis virus: insights into the structure of the coronavirion. *Proc. Natl. Acad. Sci. USA* **106**, 582–587.

Beevers, C. A., Lipson, H. (1936). A numerical method for two-dimensional Fourier synthesis. *Nature* **137**, 825–826.

Bogan, M. J., Benner, W. H., Boutet, S., Rohner, U., Frank, M., Barty, A., et al. (2008). Single particle X-ray diffractive imaging. *Nano Lett.* **8**, 310–316.

Böttcher, B., Wynne, S. A., Crowther, R. A. (1997). Determination of the fold of the core protein of hepatitis B virus by electron cryomicroscopy. *Nature* **386**, 88–91.

Bragg, W. L. (1913). The structure of some crystals as indicated by their diffraction of X-rays. *Proc. R. Soc. Lond.* **A89**, 248–277.

Bragg, W. L. (1929). The determination of parameters in crystal structures by means of Fourier series. *Proc. R. Soc. Lond.* **A123**, 537–559.

Briggs, J. A., Grunewald, K., Glass, B., Forster, F., Krausslich, H. G., Fuller, S. D. (2006). The mechanism of HIV-1 core assembly: insights from three-dimensional reconstructions of authentic virions. *Structure* **14**, 15–20.

Brünger, A. T. (1992). Free *R* value: a novel statistical quantity for assessing the accuracy of crystal structures. *Nature* **355**, 472–475.

Cheng, R. H., Kuhn, R. J., Olson, N. H., Rossmann, M. G., Choi, H. K., Smith, T. J., et al. (1995). Nucleocapsid and glycoprotein organization in an enveloped virus. *Cell* **80**, 621–630.

Cherrier, M. V., Kaufmann, B., Nybakken, G. E., Lok, S.-M., Warren, J. T., Chen, B. R., et al. (2009). Structural basis for the preferential recognition of immature flaviviruses by a fusion-loop antibody. *EMBO J.* **28**, 3269–3276.

Clare, D. K., Orlova, E. V. (2010). 4.6 Å Cryo-EM reconstruction of tobacco mosaic virus from images recorded at 300 keV on a $4k \times 4k$ CCD camera. *J. Struct. Biol.* **171**, 303–308.

Conway, J. F., Cheng, N., Zlotnick, A., Wingfield, P. T., Stahl, S. J., Steven, A. C. (1997). Visualization of a 4-helix bundle in the hepatitis B virus capsid by cryo-electron microscopy. *Nature* **386**, 91–94.

Crowfoot, D. (1948). X-ray crystallographic studies of compounds of biochemical interest. *Annu. Rev. Biochem.* **17**, 115–146.

Crowther, R. A., Amos, L. A. (1972). Three-dimensional image reconstructions of some small spherical viruses. *Cold Spring Harb. Symp. Quant. Biol.* **36**, 489–494.

Crowther, R. A., Amos, L. A., Finch, J. T., DeRosier, D. J., Klug, A. (1970). Three-dimensional reconstructions of spherical viruses by Fourier synthesis from electron micrographs. *Nature* **226**, 421–425.

Cyrklaff, M., Risco, C., Fernández, J. J., Jiménez, M. V., Estéban, M., Baumeister, W., et al. (2005). Cryo-electron tomography of vaccinia virus. *Proc. Natl. Acad. Sci. USA* **102**, 2772–2777.

Danev, R., Glaeser, R. M., Nagayama, K. (2009). Practical factors affecting the performance of a thin-film phase plate for transmission electron microscopy. *Ultramicroscopy* **109**, 312–325.

De Carlo, S., El-Bez, C., Alvarez-Rúa, C., Borge, J., Dubochet, J. (2002). Cryo-negative staining reduces electron-beam sensitivity of vitrified biological particles. *J. Struct. Biol.* **138**, 216–226.

De Carlo, S., Harris, J. R. (2011). Negative staining and cryo-negative staining of macromolecules and viruses for TEM. *Micron* **42,** 117–131.

De Rosier, D. J., Klug, A. (1968). Reconstruction of three dimensional structures from electron micrographs. *Nature* **217**, 130–134.

Dokland, T., McKenna, R., Sherman, D. M., Bowman, B. R., Bean, W. F., Rossmann, M. G. (1998). Structure determination of the ϕX174 closed procapsid. *Acta Crystallogr. D Biol. Crystallogr.* **54**, 878–890.

Dubochet, J., Adrian, M., Chang, J. J., Homo, J. C., Lepault, J., McDowall, A. W., et al. (1988). Cryo-electron microscopy of vitrified specimens. *Q. Rev. Biophys.* **21**, 129–228.

Ewald, P. P. (Ed.) (1962). Fifty Years of X-Ray DiffractionN.V.A. Oosthoek's Uitgeversmaatschappij for the International Union of Crystallography, Utrecht, The Netherlands.

Förster, F., Medalia, O., Zauberman, N., Baumeister, W., Fass, D. (2005). Retrovirus envelope protein complex structure *in situ* studied by cryo-electron tomography. *Proc. Natl. Acad. Sci. USA* **102**, 4729–4734.

Frangakis, A. S., Böhm, J., Förster, F., Nickell, S., Nicastro, D., Typke, D., et al. (2002). Identification of macromolecular complexes in cryoelectron tomograms of phantom cells. *Proc. Natl. Acad. Sci. USA* **99**, 14153–14158.

Frank, J. (1989). Image analysis of single macromolecules. *Electron Microsc. Rev.* **2**, 53–74.

Frank, J. (Ed.) (2006). Electron Tomography: Methods for Three-Dimensional Visualization of Structures in the Cell, second ed. Springer Science + Business Media, LLC, New York, NY.

Freiberg, A. N., Sherman, M. B., Morais, M. C., Holbrok, M. R., Watowich, S. J. (2008). Three-dimensional organization of Rift Valley fever virus revealed by cryo-electron tomography. *J. Virol.* **82**, 10341–10348.

Hadfield, A., Hajdu, J., Chapman, M. S., Rossmann, M. G. (1995). Laue diffraction studies of human rhinovirus 14 and canine parvovirus. *Acta Crystallogr. D Biol. Crystallogr.* **51**, 859–870.

Hafenstein, S., Bowman, V. D., Chipman, P. R., Bator Kelly, C. M., Lin, F., Medof, D. E., et al. (2007). The interaction of decay-accelerating factor with coxsackievirus B3. *J. Virol.* **81**, 12927–12935.

Harris, A., Cardone, G., Winkler, D. C., Heymann, J. B., Brecher, M., White, J. M., et al. (2006). Influenza virus pleiomorphy characterized by cryoelectron tomography. *Proc. Natl. Acad. Sci. USA* **103**, 19123–19127.

Harrison, S. C. (2010). Virology. Looking inside adenovirus. *Science* **329**, 1026–1027.

Harrison, S. C., Strong, R. K., Schlesinger, S., Schlesinger, M. T. (1992). Crystallization of Sindbis virus and its nucleocapsid. *J. Mol. Biol.* **226**, 277–280.

Hart, R. G. (1968). Electron microscopy of unstained biological material: the polytropic montage. *Science* **159**, 1464–1467.

Hayashida, M., Terauchi, S., Fujimoto, T. (2010). Automatic coarse-alignment for TEM tilt series of rod-shaped specimens collected with a full angular range. *Micron* **41**, 540–545.

Hepojoki, J., Strandin, T., Vaheri, A., Lankinen, H. (2010). Interactions and oligomerization of hantavirus glycoproteins. *J. Virol.* **84**, 227–242.

Heymann, J. A. W., Hayles, M., Gestmann, I., Giannuzzi, L. A., Lich, B., Subramaniam, S. (2006). Site-specific 3D imaging of cells and tissues with a dual beam microscope. *J. Struct. Biol.* **155**, 63–73.

Heymann, J. A. W., Shi, D., Kim, S., Bliss, D., Milne, J. L. S., Subramaniam, S. (2009). 3D imaging of mammalian cells with ion-abrasion scanning electron microscopy. *J. Struct. Biol.* **166**, 1–7.

Hogle, J. M., Chow, M., Filman, D. J. (1985). Three-dimensional structure of poliovirus at 2.9 Å resolution. *Science* **229**, 1358–1365.

Hoppe, W., Gassmann, J., Hunsmann, N., Schramm, H. J., Sturm, M. (1974). Three-dimensional reconstruction of individual negatively stained yeast fatty-acid synthetase molecules from tilt series in the electron microscope. *Hoppe-Seyler's Z. Physiol. Chem.* **355**, 1482–1487.

Huiskonen, J. T., Hepojoki, J., Laurinmäki, P., Vaheri, A., Lankinen, H., Butcher, S. J., et al. (2010). Electron cryotomography of Tula hantavirus suggests a unique assembly paradigm for enveloped viruses. *J. Virol.* **84**, 4889–4897.

Iancu, C. V., Wright, E. R., Benjamin, J., Tivol, W. F., Dias, D. P., Murphy, G. E., et al. (2005). A ''flip-flop'' rotation stage for routine dual-axis electron cryotomography. *J. Struct. Biol.* **151**, 288–297.

Jiang, W., Baker, M. L., Jakana, J., Weigele, P. R., King, J., Chiu, W. (2008). Backbone structure of the infectious ε15 virus capsid revealed by electron cryomicroscopy. *Nature* **451**, 1130–1134.

Kaufmann, B., Plevka, P., Kuhn, R. J., Rossmann, M. G. (2010). Crystallization and preliminary X-ray diffraction analysis of West Nile virus. *Acta Crystallogr.* **F66**, 558–562.

Kawase, N., Kato, M., Nishioka, H., Jinnai, H. (2007). Transmission electron microtomography without the ''missing wedge'' for quantitative structural analysis. *Ultramicroscopy* **107**, 8–15.

Kendrew, J. C., Bodo, G., Dintzis, H. M., Parrish, R. G., Wyckoff, H., Phillips, D. C. (1958). A three-dimensional model of the myoglobin molecule obtained by X-ray analysis. *Nature* **181**, 662–666.

Kendrew, J. C., Dickerson, R. E., Strandberg, B. E., Hart, R. G., Davies, D. R., Phillips, D. C., et al. (1960). Structure of myoglobin. A three-dimensional Fourier synthesis at 2 Å. resolution. *Nature* **185**, 422–427.

Kirian, R. A., Wang, X., Weierstall, U., Schmidt, K. E., Spence, J. C. H., Hunter, M., et al. (2010). Femtosecond protein nanocrystallography—data analysis methods. *Opt. Expr.* **18**, 5713–5723.

Kleywegt, G. J., Jones, T. A. (1995). Where freedom is given, liberties are taken. *Structure* **3**, 535–540.

Koster, A. J., Chen, H., Sedat, J. W., Agard, D. A. (1992). Automated microscopy for electron tomography. *Ultramicroscopy* **46**, 207–227.

Kreysing, M. K., Kießling, T., Fritsch, A., Dietrich, C., Guck, J. R., Käs, J. A. (2008). The optical cell rotator. *Opt. Expr.* **16**, 16984–16992.

Leis, A., Rockel, B., Andrees, L., Baumeister, W. (2009). Visualizing cells at the nanoscale. *Trends Biochem. Sci.* **34**, 60–70.

Liu, H., Jin, L., Koh, S. B. S., Atanasov, I., Schein, S., Wu, L., et al. (2010). Atomic structure of human adenovirus by cryo-EM reveals interactions among protein networks. *Science* **329**, 1038–1043.

Liu, X., Zhang, Q., Murata, K., Baker, M. L., Sullivan, M. B., Fu, C., et al. (2010). Structural changes in a marine podovirus associated with release of its genome into *Prochlorococcus*. *Nat. Struct. Mol. Biol.* **17**, 830–836.

Loney, C., Mottet-Osman, G., Roux, L., Bhella, D. (2009). Paramyxovirus ultrastructure and genome packaging: cryo-electron tomography of sendai virus. *J. Virol.* **83**, 8191–8197.

Lonsdale, K. (1928). The structure of the benzene ring. *Nature* **122**, 810.

Lučić, V., Förster, F., Baumeister, W. (2005). Structural studies by electron tomography: from cells to molecules. *Ann. Rev. Biochem.* **74**, 833–865.

Medalia, O., Weber, I., Frangakis, A. S., Nicastro, D., Gerisch, G., Baumeister, W. (2002). Macromolecular architecture in eukaryotic cells visualized by cryoelectron tomography. *Science* **298**, 1209–1213.

Milazzo, A.-C., Moldovan, G., Lanman, J., Jin, L., Bouwer, J. C., Klienfelder, S., et al. (2010). Characterization of a direct detection device imaging camera for transmission electron microscopy. *Ultramicroscopy* **110**, 744–747.

Murata, K., Liu, X., Danev, R., Jakana, J., Schmid, M. F., King, J., et al. (2010). Zernike phase contrast cryo-electron microscopy and tomography for structure determination at nanometer and subnanometer resolutions. *Structure* **18**, 903–912.

Olson, N. H., Kolatkar, P. R., Oliveira, M. A., Cheng, R. H., Greve, J. M., McClelland, A., et al. (1993). Structure of a human rhinovirus complexed with its receptor molecule. *Proc. Natl. Acad. Sci. USA* **90**, 507–511.

Ortiz, J. O., Förster, F., Kürner, J., Linaroudis, A. A., Baumeister, W. (2006). Mapping 70S ribosomes in intact cells by cryoelectron tomography and pattern recognition. *J. Struct. Biol.* **156**, 334–341.

Overby, A. K., Pettersson, R. F., Grünewald, K., Huiskonen, J. T. (2008). Insights into bunyavirus architecture from electron cryotomography of Uukuniemi virus. *Proc. Natl. Acad. Sci. USA* **105**, 2375–2379.

Patterson, A. L. (1934). A Fourier series method for the determination of the components of interatomic distances in crystals. *Phys. Rev.* **46**, 372–376.

Patterson, A. L. (1935). A direct method for the determination of the components of interatomic distances in crystals. *Z. Kristallogr.* **90**, 517–542.

Perutz, M. F., Rossmann, M. G., Cullis, A. F., Muirhead, H., Will, G., North, A. C. T. (1960). Structure of haemoglobin. A three-dimensional Fourier synthesis at 5.5-Å resolution, obtained by X-ray analysis. *Nature* **185**, 416–422.

Rosenthal, P. B., Henderson, R. (2003). Optimal determination of particle orientation, absolute hand, and contrast loss in single-particle electron cryomicroscopy. *J. Mol. Biol.* **333**, 721–745.

Rossmann, M. G. (2000). Fitting atomic models into electron microscopy maps. *Acta Crystallogr. D Biol. Crystallogr.* **56**, 1341–1349.

Rossmann, M. G. and Arnold, E. (Eds.) (2001). International Tables for Crystallography Volume F: Crystallography of Biological Macromolecules. Kluwer Academic Publishers for International Union of Crystallography, Dordrecht, The Netherlands.

Rossmann, M. G., Arnold, E., Erickson, J. W., Frankenberger, E. A., Griffith, J. P., Hecht, H. J., et al. (1985). Structure of a human common cold virus and functional relationship to other picornaviruses. *Nature* **317**, 145–153.

Rossmann, M. G., Bernal, R., Pletnev, S. V. (2001). Combining electron microscopic with X-ray crystallographic structures. *J. Struct. Biol.* **136**, 190–200.

Rossmann, M. G., Leslie, A. G. W., Abdel-Meguid, S. S., Tsukihara, T. (1979). Processing and post-refinement of oscillation camera data. *J. Appl. Crystallogr.* **12**, 570–581.

Scheres, S. H. W., Gao, H., Valle, M., Herman, G. T., Eggermont, P. P. B., Frank, J., et al. (2007). Disentangling conformational states of macromolecules in 3D-EM through likelihood optimization. *Nat. Methods* **4**, 27–29.

Smith, T. J., Olson, N. H., Cheng, R. H., Liu, H., Chase, E. S., Lee, W. M., et al. (1993). Structure of human rhinovirus complexed with Fab fragments from a neutralizing antibody. *J. Virol.* **67**, 1148–1158.

Suloway, C., Pulokas, J., Fellmann, D., Cheng, A., Guerra, F., Quispe, J., et al. (2005). Automated molecular microscopy: the new Leginon system. *J. Struct. Biol.* **151**, 41–60.

Taylor, D. J., Devkota, B., Huang, A. D., Topf, M., Narayanan, E., Sali, A., et al. (2009). Comprehensive molecular structure of the eukaryotic ribosome. *Structure* **17**, 1591–1604.

Tong, L., Rossmann, M. G. (1997). Rotation function calculations with GLRF program. *Methods Enzymol.* **276**, 594–611.

Unwin, P. N. T., Henderson, R. (1975). Molecular structure determination by electron microscopy of unstained crystalline specimens. *J. Mol. Biol.* **94**, 425–440.

van Heel, M., Schatz, M. (2005). Fourier shell correlation threshold criteria. *J. Struct. Biol.* **151**, 250–262.

Volkmann, N. (2009). Confidence intervals for fitting of atomic models into low-resolution densities. *Acta Crystallogr. D Biol. Crystallogr.* **65**, 679–689.

Volkmann, N., Hanein, D. (2003). Docking of atomic models into reconstructions from electron microscopy. *Methods Enzymol.* **374**, 204–225.

Wikoff, W. R., Wang, G., Parrish, C. R., Cheng, R. H., Strassheim, M. L., Baker, T. S., et al. (1994). The structure of a neutralized virus: canine parvovirus complexed with neutralizing antibody fragment. *Structure* **2**, 595–607.

Yu, X., Jin, L., Zhou, Z. H. (2008). 3.88 Å structure of cytoplasmic polyhedrosis virus by cryo-electron microscopy. *Nature* **453**, 415–419.

Zanetti, G., Briggs, J. A., Grünewald, K., Sattentau, Q. J., Fuller, S. D. (2006). Cryo-electron tomographic structure of an immunodeficiency virus envelope complex in situ. *PLoS Pathog.* **2**(8), e83.

Zhang, X., Jin, L., Fang, Q., Hui, W. H., Zhou, Z. H. (2010). 3.3 Å cryo-EM structure of a nonenveloped virus reveals a priming mechanism for cell entry. *Cell* **141**, 472–482.

Zhang, Y., Zhang, W., Ogata, S., Clements, D., Strauss, J. H., Baker, T. S., et al. (2004). Conformational changes of the flavivirus E glycoprotein. *Structure* **12**, 1607–1618.

Zhu, P., Liu, J., Bess, J., Jr., Chertova, E., Lifson, J. D., Grisé, H., et al. (2006). Distribution and three-dimensional structure of AIDS virus envelope spikes. *Nature* **441**, 847–852.